

Viral infection in internally structured hosts. I. Conditions for persistent infection

Maria E. Orive^{a,*}, Miles N. Stearns^a, John K. Kelly^a, Michael Barfield^b,
Marilyn S. Smith^c, Robert D. Holt^b

^a*Department of Ecology and Evolutionary Biology, University of Kansas, 1200 Sunnyside Ave., Lawrence, KS 66045, USA*

^b*Department of Zoology, University of Florida, 223 Bartram Hall, PO Box 118525, Gainesville, FL 32611, USA*

^c*Department of Microbiology, Molecular Genetics, and Immunology, University of Kansas Medical Center, Kansas City, KS 66160, USA*

Received 27 August 2003; received in revised form 14 July 2004; accepted 23 August 2004

Available online 8 October 2004

Abstract

For a virus population within its host, two important levels of structure can be considered: multiple cell types which can be infected, and tissue types or body compartments which may be coupled via movement. We develop a model with both types of structure. Migration between compartments can create “sources” and “sinks” within the virus population, where realized viral growth rate and abundance is lowered in some compartments compared to what would be observed in isolation. Using both analytical and numerical methods, we investigate how this within-host spatial structure affects the conditions for persistent viral infection. We find that migration between compartments makes the establishment of infection more difficult than it would be in the absence of migration, implying that within-host spatial structure combined with viral movement decreases the likelihood of viral establishment. If migration is symmetrical and compartments are heterogeneous, an increase in migration rates between compartments generally makes establishment less likely. This may help to explain the tissue specificity observed for many viruses. There are, however, important exceptions to this result. These include circumstances where the virus initially invades a compartment that is unfavorable to population growth and migration is necessary to infect other parts of the host body. Stochastic aspects of viral establishment may also favor increased migration as it tends to dampen the amplitude of fluctuations in population size during the initial transient phase of establishment.

© 2004 Elsevier Ltd. All rights reserved.

Keywords: HIV; Viral dynamics; Population structure

1. Introduction

For an infecting virus, the vertebrate host represents a large, complex, spatially structured landscape, with different cell types and tissue types potentially acting as different “habitats” that are connected via dispersal. There are strong empirical grounds for examining the consequences of this internal structure for pathogen dynamics. For instance, work on HIV has found substantial genetic differentiation among virus populations in different organs (Delassus et al., 1992; Epstein

et al., 1991; Pang et al., 1991; Wang et al., 2001). This differentiation may be due to sampling error caused by small numbers of virions initially invading any particular body compartment (genetic drift), or by compartment-specific selection on viral variants. But in any case, it is unlikely that such genetic differences will persist without substantial among-organ compartmentalization of viral dynamics.

Evidence for within-host spatial structure in viral populations is intriguing in light of the growing appreciation in ecology (Tilman and Kareiva, 1997), evolutionary biology (Hanski and Gilpin, 1997; Wade and Goodnight, 1998), and epidemiology (Andreasen and Christiansen, 1989; May and Anderson, 1990;

*Corresponding author. Tel.: 785 864 3763; fax: 785 864 5321.

E-mail address: morive@ku.edu (M.E. Orive).

Dobson and Foufopoulos, 2001; May et al., 2001; Fulford et al., 2002) of the critical importance of spatial structuring for explaining species persistence and the direction of evolutionary change. Space can affect persistence in several ways. For instance, in homogeneous but spatially distributed environments, locally unstable interactions (e.g., predator–prey) may persist because of spatial separation, which permits different areas to be in different dynamical phases (Hassell et al., 1994; Tilman, 1994). Moreover, there is often spatial variability in local factors affecting population growth. For example, in ecology, spatial refuges often appear essential for explaining persistence of strong predator–prey or host–parasitoid interactions (e.g., Holt and Hassell, 1993). The interaction between virus and cells of the immune system shares many features with predator–prey systems (Nowak and May, 2000). Holt (2000) outlines numerous conceptual parallels between contemporary spatial ecology and within-host infection processes. Several models of the effects of spatial heterogeneity on the spread of disease (Andreasen and Christiansen, 1989; May and Anderson, 1990; May et al., 2001) show that, for a host population partitioned into subpopulations, with some proportion of contacts between hosts (and thus transmission of the parasite or pathogen) occurring within a subpopulation and some between populations, disease persistence can occur via two avenues. Either the basic reproductive rate of the parasite or pathogen within the subgroup may be sufficiently high, or disease transmission between subgroups may be sufficiently high for the disease to persist via spread between subgroups. However, Andreasen and Christiansen (1989) found that, if the disease cannot exist in any of the subpopulations alone ($R_{0i} < 1$ for all subpopulations i) increasing the inter-population contact probability (migration rate) alone, without increasing the within-population contact probability (transmission rate) could not make the disease persist.

In recent years, a rich literature has arisen developing a quantitative theory of the within-host population dynamics of infections (e.g., McLean and Nowak, 1992; Antia et al., 1994; Bonhoeffer et al., 1997; Essunger and Perelson, 1994; Herz et al., 1996; Perelson, 1989; Perelson et al., 1993; Perelson et al., 1996; Tuckwell and Le Corfec, 1998; Kirschner et al., 1998; Lipsitch and Levin, 1997, 1998; Kepler and Perelson, 1998; Solé et al., 1999; Hlavacek et al., 2000; Nelson et al., 2000; Kirschner, 2001; Nelson and Perelson, 2002; Ribeiro et al., 2002; Verotta and Schaedeli, 2002). Our approach differs from these by focusing explicitly on within-host spatial and cell structure and the effects of such structure on viral population and evolutionary dynamics. Our models consider multiple cell-type and free virus populations, as well as spatial heterogeneity imposed by the existence of within-host compartments

coupled by viral and cell movement via fluid flow. Parameters determining the relationships among various within-host populations, defined by the pattern and rates of coupling between compartments, are explicitly included. These ingredients are all necessary to examine the consequences of internal host spatial structure for viral dynamics.

There are two complementary aspects of population structure that in principle can be incorporated into within-host models. First, within any given tissue compartment, there may be multiple cell types which can be infected, as well as free virus. A “minimal” model would include uninfected cells, infected cells, and free virus. Such models can be made more elaborate; for example, for HIV infection, an expanded model might include additional cell states (e.g., latency) or cell types (e.g., macrophages). For instance, Perelson et al. (1997) show that the temporal dynamics of viral load after initiation of drug treatment involve multiple phases of decay, reflecting different cell types with differing loss rates (see also Kelly, 1996). Second, as noted above, a host individual in effect is comprised of a suite of local “habitats” coupled by fluid flow and cell movement. Several authors have begun to examine the implications of within-host spatial structure for infection dynamics. For instance, Kirschner et al. (1998) develop a model in which the thymus is coupled with the blood. The model includes the transport of cells and virus between the blood and a lymphoid compartment. They showed that this coupling could lead to an augmentation of overall viral load. Kepler and Perelson (1998) explored a model in which drugs have different concentrations in different spatial compartments, and analyse the evolution of resistance. They conclude that spatial heterogeneity may significantly increase the likelihood of evolved resistance. Stekel (1997) studied a model of lymphocyte circulation, highlighting the importance of movement among compartments. Callaway and Perelson (2002), in a paper examining the ability of different mathematical models to explain sustained low viral loads of HIV-1 during highly active antiretroviral therapy (HAART), considered a model with two physiologically distinct compartments, one of which acted as a “drug sanctuary.” If the source of virus during therapy was the drug sanctuary, they found that viral load rapidly reached steady state, but oscillated in the process. They hypothesized that these oscillations might provide a possible explanation for intermittent episodes of detectable viremia observed in patients whose viral load is otherwise suppressed. In a recent study, Cuevas et al. (2003) developed a model which followed viral genotypes in various tissue types (environments); simulation results predicted that increased migration between tissues should decrease the abundance of locally favored genotypes by removing these genotypes from their “best” environment. Experimental *in vitro* tests of this

model using mammalian cell cultures supported these predictions, implying that migration among heterogeneous cell environments should select for generalist viruses and against specialization.

Our own work has recently linked viral population dynamics and population genetics by focusing on a “standard model” of viral dynamics, generalized to consider the infection of multiple host cell types (Kelly et al., 2003). This model is similar to that of Nowak and May (2000), except that we include a term representing the loss of a free virion each time a cell is newly infected. The other difference is in virion production. We specify virion production rate by an infected cell as the product of infected cell death rate and burst size while Nowak and May (2000) use a single parameter for this product. We found that, while the inclusion of multiple cell types increases the likelihood of persistent infection and can increase the amount of genetic diversity within the viral population, it may actually decrease the overall rate of viral gene sequence evolution. In this paper, we extend our previous model, which considered only cellular population structure, to a model that considers both cellular population structure and spatial compartment structure. We use this model to ask the first of two important ecological questions: How does this additional level of within-host structure affect the conditions for persistent infection? A follow-up paper will answer the linked question of how such structure impacts the equilibrium levels of virus load and numbers of infected cells. The ecological results presented here will provide a springboard for future analyses of coupled evolutionary and population dynamics.

2. Model

2.1. General model

We begin by considering a dynamical model with an arbitrary number of target cells and an arbitrary number of compartments. The dynamical variables followed include the number of virions in each compartment i (q_i), and the number of uninfected (n_{ji}) and infected (n_{ji}^*) cells of each type j and compartment i . We assume that movement between compartments can occur via migration of virions, cells, or both virions and cells. Changes in these quantities are described by the following system of differential equations (Table 1 summarizes the model variables and parameters):

$$\frac{dq_i}{dt} = \sum_j \mu_{ji}^* v_{ji} n_{ji}^* - \mu_i' q_i - \sum_j \beta_{ji} n_{ji} q_i + \sum_{k \neq i} m_{ki} q_k - \sum_{k \neq i} m_{ik} q_i, \quad (1)$$

Table 1
Variables and Parameters

Dynamical variables

q_i = number of virions in compartment i
 n_{ji} = number of uninfected cells of type j in compartment i
 n_{ji}^* = number of infected cells of type j in compartment i

Constants

[For the following constants, the subscript j gives the cell type, and i indicates the within-host compartment. In the text, the j subscript is generally dropped when there is only one cell type.]

v_{ji} = burst size, the number of virions produced from an infected cell
 λ_{ji} = input rate of uninfected cells
 μ_{ji} = death rate of uninfected cells
 μ_{ji}^* = death rate of infected cells
 μ_i' = death rate of virions (clearance rate by host immune system)
 β_{ji} = infection constant
 m_{ik} = migration rate of virions from compartment i to compartment k
 M_{ik} = migration rate of uninfected cells from compartment i to compartment k
 M_{ik}^* = migration rate of infected cells from compartment i to compartment k

$$\frac{dn_{ji}}{dt} = \lambda_{ji} - \mu_{ji} n_{ji} - \beta_{ji} n_{ji} q_i + \sum_{k \neq i} M_{ki} n_{jk} - \sum_{k \neq i} M_{ik} n_{ji}, \quad (2)$$

$$\frac{dn_{ji}^*}{dt} = \beta_{ji} n_{ji} q_i - \mu_{ji}^* n_{ji}^* + \sum_{k \neq i} M_{ki}^* n_{jk}^* - \sum_{k \neq i} M_{ik}^* n_{ji}^*, \quad (3)$$

where j indicates the cell type, i indicates the compartment, v_{ji} gives the “burst size” (number of virions released when an infected cell dies; $v_{ji} - 1$ will sometimes be referred to as “net burst size”), μ_i' is the death rate of virions (clearance rate), β_{ji} is the infection constant, λ_{ji} is the input rate of uninfected cells, μ_{ji} is the death rate of uninfected cells, μ_{ji}^* is the death rate of infected cells, and m_{ik} , M_{ik} , M_{ik}^* give the migration rates of virions, uninfected cells and infected cells from compartment i to compartment k . The sum over j is for cell types, while the sum over k is for compartments. (Note that we assume that cell migration rates are not cell-type specific; to include this further level of detail, one would need to indicate an additional subscript j for the M and M^* migration terms.)

2.2. Conditions for infection: a single compartment

The conditions for infection with one compartment are of course well known, and can be derived using the basic reproductive ratio (R_0), which is the expected number of free virions produced by infection caused by a single virion, when virions (and infected cells) are very rare. If the infection is rare, the uninfected cell number for each cell type will approach the no-infection equilibrium $\hat{n}_{j1} = \lambda_{j1} / \mu_{j1}$. Free virions are cleared

(producing no new virions) at a rate μ'_1 and infect cells of type j (resulting in v_{j1} new virions) at a rate of $\hat{n}_{j1}\beta_{j1}$. Of these possible outcomes, only one can occur for a given virion, and the probability of each is that event's rate divided by the total rate of all possible events (assuming all are Poisson processes). So the probability that a virion is cleared is $\mu'_1/(\mu'_1 + \sum \beta_{j1}\hat{n}_{j1})$ while the probability that it infects a cell of type j is $\beta_{j1}\hat{n}_{j1}/(\mu'_1 + \sum \beta_{j1}\hat{n}_{j1})$. Weighting the number of virions produced by each event (0 or v_{j1}) by its probability gives $R_0 = \sum \beta_{j1}\hat{n}_{j1}v_{j1}/(\mu'_1 + \sum \beta_{j1}\hat{n}_{j1})$. For the virus to increase when rare, $R_0 > 1$, which requires $\sum \beta_{j1}\hat{n}_{j1}v_{j1} > \mu'_1 + \sum \beta_{j1}\hat{n}_{j1}$, implying that $\sum \beta_{j1}\hat{n}_{j1}(v_{j1} - 1) > \mu'_1$.

The corresponding equation for R_0 from Nowak and May (2000), extended to multiple cell types, is $R_0 = \sum \beta_{j1}\hat{n}_{j1}v_{j1}/\mu'_1$. The difference arises because we include a term for uptake of a virion when a cell becomes infected. Therefore, a single virion can only infect one cell. The two formulations are approximately equivalent if $\mu'_1 \gg \sum \beta_{j1}\hat{n}_{j1}$, which means that the great majority of virions are cleared before infecting a cell, as is probably often true.

2.3. Conditions for infection: Two compartments

In Appendix A, we derive conditions for increase of the virus when rare for some limiting cases of the above general model. The general model is too complex for a complete analytic treatment, so we begin by considering the special case of one cell type and two compartments (we therefore drop the subscript indicating cell type in this section). As an example, for HIV, we might consider T cells in both lymph nodes (compartment 1) and blood (compartment 2). The dynamical variables followed include the number of virions in each compartment (q_1 and q_2), the number of uninfected cells in each compartment (n_1 and n_2), and the number of infected cells in each compartment (n_1^* and n_2^*). Changes in these quantities are described by the following system of differential equations (a simpler version of Eqs. (1)–(3)):

$$\frac{dq_1}{dt} = \mu_1^*v_1n_1^* - \mu'_1q_1 - \beta_1n_1q_1 + m_{21}q_2 - m_{12}q_1, \tag{4}$$

$$\frac{dq_2}{dt} = \mu_2^*v_2n_2^* - \mu'_2q_2 - \beta_2n_2q_2 - m_{21}q_2 + m_{12}q_1, \tag{5}$$

$$\frac{dn_i}{dt} = \lambda_i - \mu_i n_i - \beta_i n_i q_i + M_{ki} n_k - M_{ik} n_i, \tag{6}$$

$$\frac{dn_i^*}{dt} = \beta_i n_i q_i - \mu_i^* n_i^* + M_{ki}^* n_k^* - M_{ik}^* n_i^*, \tag{7}$$

where $i = 1, 2$ and $k = 2, 1$ indicate the compartment [so there are a total of 6 equations, with 2 each of the form of Eqs. (6) and (7)].

The first question we address is whether or not the infection can become established. Does migration ever

make it easier for the virus to initially become established? The condition for the virus to increase when rare can be found by evaluating the eigenvalues at the ‘‘edge’’ equilibrium at which virions and infected cells are at 0, and uninfected cells are at their infection-free equilibrium. We carry out this analysis for the two simpler cases of viral migration alone and cell migration alone (the more complex case with both viral and cell migration is considered numerically below).

As shown in Appendix B, under viral migration alone ($M_{ik}^*, M_{ik} = 0$), the virus increases when rare (at a sufficiently low level that uninfected cell numbers can be assumed to be constant at their no-infection equilibrium) if

$$[\mu'_1 + m_{12} - \hat{n}_1\beta_1(v_1 - 1)][\mu'_2 + m_{21} - \hat{n}_2\beta_2(v_2 - 1)] - m_{12}m_{21} < 0, \text{ or} \tag{8a}$$

$$\mu'_1 + m_{12} - \hat{n}_1\beta_1(v_1 - 1) < 0, \text{ or} \tag{8b}$$

$$\mu'_2 + m_{21} - \hat{n}_2\beta_2(v_2 - 1) < 0, \tag{8c}$$

where $\hat{n}_i = \lambda_i/\mu_i$ is the equilibrium number of uninfected cells in the absence of virus. Relation (8a) determines the boundary for viral increase (see below). [Relations (8a), (8b) and (8c) and the analysis that follows would also apply if the uninfected cell equations were changed (for example, to reflect logistic growth), as long as, in the absence of infection, uninfected cells reached a stable equilibrium (with \hat{n}_i being the equilibrium).]

Notice that the death rate for infected cells (μ_i^* , which must be positive) does not affect the initial establishment of the viral infection, although it does affect the rate of increase of virus once infection has been established. This seems to be a general feature of many comparable models (see Kelly et al., 2003). This conclusion depends on our specification of virion production rate as the product of infected cell death rate and burst size. In Nowak and May (2000), with virion production rate independent of infected cell death rate, the latter does affect the ability of the virus to increase when rare (since it determines the average time over which an infected cell produces virions, which are produced at a fixed rate, rather than a fixed number per infected cell).

In inequality (8a), the two factors in brackets consist of positive terms related to loss of virions (clearance and emigration), and a negative term related to the production of virions (infection rate per virion, $\hat{n}_i\beta_i$, multiplied by net burst size, $v_i - 1$). For very low infection rate or burst size, the factors in brackets are both positive and all inequalities in Eq. (8) are false, so the virus cannot increase when rare. As infection rate or burst size is increased, eventually the first inequality is satisfied and the virus can increase when rare. With further increases, both of the bracketed factors eventually become negative and the first inequality eventually again

becomes false. However, at this point the virus can still increase when rare. (For details, see Appendix B.)

Relation (8) was derived by evaluating the stability of the equilibrium of Eqs. (4)–(7) with infected cells and virions at zero density. An alternative is to calculate the value of R_0 , which is derived for a two-compartment, multiple-cell-type system in Appendix A. The condition $R_0 > 1$ gives the same conditions as Eq. (8).

As shown in Appendix B, under cell migration (and in the absence of viral migration, $m_{ik} = 0$), the condition for viral increase when rare is

$$\left[\mu_1^* + M_{12}^* - \frac{\mu_1^* v_1 \beta_1 \hat{n}_1}{\mu_1' + \beta_1 \hat{n}_1} \right] \left[\mu_2^* + M_{21}^* - \frac{\mu_2^* v_2 \beta_2 \hat{n}_2}{\mu_2' + \beta_2 \hat{n}_2} \right] - M_{12}^* M_{21}^* < 0, \text{ or} \tag{9a}$$

$$\mu_1^* + M_{12}^* - \frac{\mu_1^* v_1 \beta_1 \hat{n}_1}{\mu_1' + \beta_1 \hat{n}_1} < 0, \text{ or} \tag{9b}$$

$$\mu_2^* + M_{21}^* - \frac{\mu_2^* v_2 \beta_2 \hat{n}_2}{\mu_2' + \beta_2 \hat{n}_2} < 0, \tag{9c}$$

where \hat{n}_i is the equilibrium number of uninfected cells in the absence of virus,

$$\hat{n}_i = \frac{\mu_k \lambda_i + M_{ki}(\lambda_i + \lambda_k)}{\mu_i \mu_k + \mu_i M_{ki} + \mu_k M_{ik}}$$

and $i = 1, 2$ and $k = 2, 1$ again indicate the compartment. Unlike the case for viral movement, here the death rate for infected cells (μ_i^*) does affect the initial establishment of the virus (since it affects the probability of an infected cell moving from one compartment to another before dying). The above relations can be expressed in terms of M_{ik}^*/μ_i^* , so only the relative values of infected cell migration and death rates determine whether the virus can increase when rare.

Uncoupled compartments: Consider the limiting case of viral and cell migration (in both directions) being set to zero, so that the two compartments are decoupled. Then, the condition for increase in each compartment i (from the above discussion of a one-compartment system) is simply

$$\hat{n}_i > \frac{\mu_i'}{\beta_i(v_i - 1)}. \tag{10}$$

This condition is analogous to the “minimum threshold host abundance” that is familiar from epidemiological models. The cell abundance required for viral persistence reflects infection rates, burst sizes [assumed to be greater than 1 in Eq. (10)], and virion clearance rates.

Parameter analysis: We can use Eqs. (4)–(7) to investigate the conditions for infection numerically. The Jacobian matrix corresponding to this set of equations at its no-infection equilibrium is given as expression (B1) in Appendix B. The virus can increase when rare if the dominant eigenvalue of the lower right 4×4 submatrix of this matrix is positive. Therefore, to

find values of one parameter that allow the virus to increase when rare, we assign numerical values to all other parameters and set the numbers of uninfected cells to their equilibrium values in the absence of infection, $\hat{n}_i = [\mu_k \lambda_i + M_{ki}(\lambda_i + \lambda_k)]/(\mu_i \mu_k + \mu_i M_{ki} + \mu_k M_{ik})$. We then vary the focal parameter and determine the range of values giving a positive dominant eigenvalue as a function of cell and virion migration rates. For all cases with coupled compartments, numerical iteration of the differential equations indicates that a non-zero equilibrium for infected cells and virus occurs whenever this eigenvalue is greater than zero, as we would expect from theoretical considerations. We consider the case of two compartments and one cell type, and to simplify analysis further, allow migration to be symmetric and equal between infected and uninfected cells ($m_{12} = m_{21} = m$ and $M_{12} = M_{21} = M_{12}^* = M_{21}^* = M$).

We first find the critical burst size (v_{crit} , assumed equal in the two compartments) above which infection can occur and below which infection cannot occur, as a function of m and M (Fig. 1). The intersection of this surface with the $M = 0$ plane can be found by solving (8) for virion migration alone, and with the $m = 0$ plane by solving (9) for cell migration alone. With only one type of migration, the critical burst size is monotonic with migration rate (m or M), and the initial slope with respect to migration rate for v_{crit} is found to be $1/\hat{n}_i \beta_i$ for virion migration alone and $(\mu_i' + \hat{n}_i \beta_i)/(\mu_i^* \hat{n}_i \beta_i)$ for cell migration alone (where i denotes the compartment with the lower value for $\mu_i' \hat{n}_i \beta_i$). However, the critical burst size is not always monotonically increasing under both types of migration. Fig. 1 provides two numerical examples showing the critical value v_{crit} above which the dominant eigenvalue of the Jacobian matrix (B1, Appendix B) is positive and infection occurs, and below which infection cannot occur. For either viral migration alone (front right plane of Fig. 1a, front left plane of Fig. 1b) or cell migration alone (front left plane of Fig. 1a, front right plane of Fig. 1b), the critical value for burst size increases as migration between compartments increases, indicating that migration makes it more difficult for infection to occur. But when both types of migration occur, there are some cases in which adding virion migration makes infection easier (Fig. 1b). While, in Fig. 1a, the two compartments differ only in virion clearance rate ($\mu_1' < \mu_2'$), in Fig. 1b, compartment 2 is less favorable for the virus due to a higher virion clearance rate ($\mu_1' < \mu_2'$), a higher infected cell death rate ($\mu_1^* < \mu_2^*$) and a lower infection constant ($\beta_1 > \beta_2$). Here, if there is no virion migration, cell migration causes a loss of infected cells due to migration into compartment 2, where μ_2^* is high. Virions released when the infected cells die in compartment 2 tend to be cleared because of the high clearance rate (μ_2') and low infectivity (β_2). This leads to little backflow of infected cells into compartment 1 (which is more favorable for infection). Adding

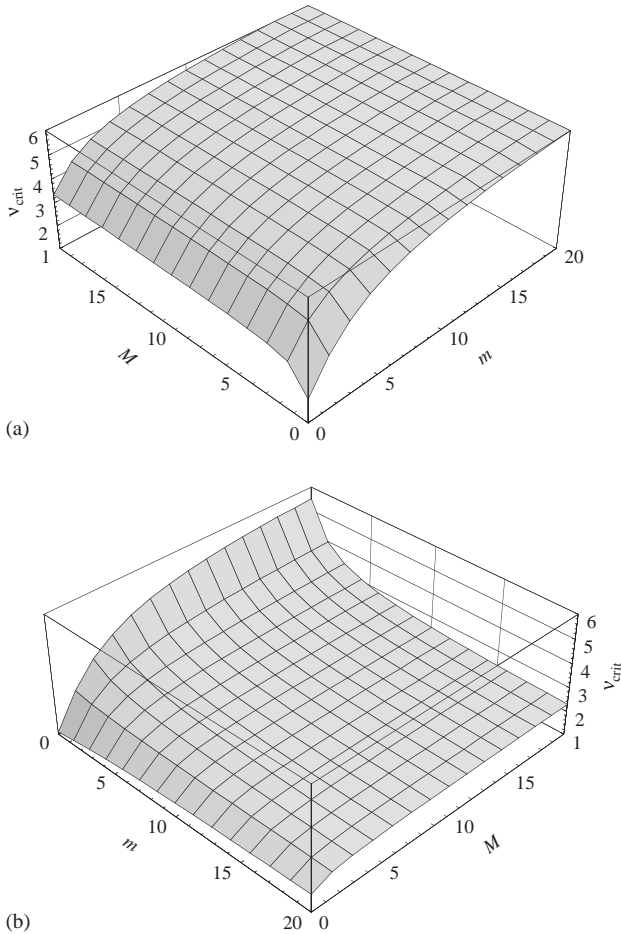


Fig. 1. Critical value of burst size (v_{crit}) for two-compartment, one-cell type model; values of v above the surface allow for infection. Migration is symmetric and assumed equal for uninfected and infected cells ($m_1 = m_2 = m$ and $M_1 = M_2 = M_1^* = M_2^* = M$). Both viral and cell migration rates range from 0 to 20. (a) Parameter values are $\lambda_1 = \lambda_2 = 10$, $\mu_1 = \mu_2 = 0.001$, $\mu_1^* = \mu_2^* = 1$, $\beta_1 = \beta_2 = 10^{-4}$, $\mu'_1 = 1$ and $\mu'_2 = 10$. (b) Parameter values are $\lambda_1 = \lambda_2 = 10$, $\mu_1 = \mu_2 = 0.001$, $\mu_1^* = 1$, $\mu_2^* = 10$, $\beta_1 = 10^{-3}$, $\beta_2 = 10^{-4}$, $\mu'_1 = 1$ and $\mu'_2 = 10$. Note that the orientation for the x and y axes (m and M) are switched between (a) and (b), so that the surface of each plot can be clearly seen.

virion migration provides another path for virus to return to the favorable compartment, and to migrate out of the unfavorable compartment prior to clearance. Thus, at higher levels of cell migration (M), the critical value for burst size decreases with increasing virion migration (m).

If we allow either migration rate alone to increase toward infinity, we find that the critical burst size approaches

$$v_{crit}(m) = 1 + \frac{\mu'_1 + \mu'_2}{\beta_1 \hat{n}_1 + \beta_2 \hat{n}_2}$$

for virion migration alone and

$$v_{crit}(M) = \frac{\mu_1^* + \mu_2^*}{(\mu_1^* \beta_1 \hat{n}_1 / \mu'_1 + \beta_1 \hat{n}_1) + (\mu_2^* \beta_2 \hat{n}_2 / \mu'_2 + \beta_2 \hat{n}_2)}$$

for cell migration alone. The critical burst size approaches the first expression above ($v_{crit}(m)$) as virion migration becomes infinite for any value of cell migration, but approaches the second expression ($v_{crit}(M)$) as cell migration becomes infinite only when virion migration is zero. These can be seen Fig. 1, where the plots for v_{crit} becomes flat at high m but not at high M . Generally, if burst sizes are the same in both compartments and the equilibrium numbers for uninfected cells are independent of M (which will be true whenever the ratio λ_i/μ_i is equal for the two compartments), at sufficiently high m , for any value of M , the condition for viral increase when rare is

$$(\beta_1 \hat{n}_1 + \beta_2 \hat{n}_2)(v - 1) > (\mu'_1 + \mu'_2). \tag{11}$$

Solving this equation for v gives the expression given above for $v_{crit}(m)$.

If we assume that input of uninfected cells, infection constants, and uninfected cell death rates are the same in both compartments, these three parameters then always appear together (as $\beta_i \hat{n}_i = \beta_i \lambda_i / \mu_i$) in the conditions for infection. Fig. 2 shows the critical value for the combined parameters $[(\beta \lambda / \mu)_{crit}]$ as a function of both viral and cell migration, where the two compartments differ in viral clearance rates ($\mu'_1 \neq \mu'_2$). A higher input of uninfected cells, a higher infection constant, and/or a lower uninfected cell death rate are needed under migration than without migration, indicating that migration makes infection more difficult under these conditions. From Eq. (11), we see that if burst sizes in the two compartments are equal, the critical value of this compound parameter again approaches a constant value at high values of virion migration (m), $(\mu'_1 + \mu'_2) / [2(v - 1)]$, which is independent of the cell migration rate (M).

Virial clearance rates (μ'_i) have a negative effect on the conditions for infection. Increasing μ'_1 and μ'_2 makes infection less likely, so that here, μ'_{crit} gives a maximum instead of a minimum value. In Fig. 3, the viral clearance rate in compartment 2 is an order of magnitude higher than the viral clearance rate in compartment 1 [$\mu'_2 = 10\mu'_1$, note that the migration rates range from 0 to 100 in (a) and from 0 to 20 in (b)]. When only the viral clearance rates differ between the two compartments (Fig. 3a), the effect of increasing migration is seen most strongly under viral migration (front left plane of Fig. 3a); as viral migration becomes very large, the clearance rate approaches the average of the clearance rates in the two compartments, which is quite high. The effect of letting one compartment be “better” in some respects for infection while “worse” in other respects can be seen in Fig. 3b. Here, the parameters are as in part (a), except that the input rates of uninfected cells also differ between compartments ($\lambda_1 = 1$, $\lambda_2 = 10$), such that the compartment with the higher viral clearance rate (compartment 2) also has a

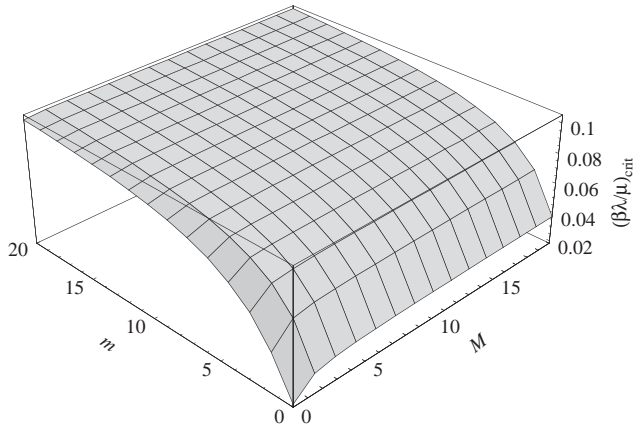


Fig. 2. Critical value for infection constant, input rate of uninfected cells, and death rate of uninfected cells $[(\beta\lambda/\mu)_{crit}]$ for two-compartment, one-cell type model; values of $\beta\lambda/\mu$ above the surface allow for infection. Parameter values are $v_1 = v_2 = 50$, $\mu_1 = \mu_2 = 0.001$, $\mu_1^* = \mu_2^* = 1$, $\beta_1 = \beta_2 = 10^{-4}$, $\mu'_1 = 1$ and $\mu'_2 = 10$. Migration is symmetric and assumed equal for uninfected and infected cells ($m_1 = m_2 = m$ and $M_1 = M_2 = M_1^* = M_2^* = M$). Both viral and cell migration rates range from 0 to 20.

higher input rate of uninfected cells. Increased viral migration still makes infection less likely, but increased cell migration initially makes infection more likely, with a very rapid increase in μ'_{crit} as M increases from zero. This is because cell migration “rescues” the compartment with low uninfected cell recruitment, by allowing migration of uninfected cells. The equilibrium values of uninfected cells with no migration are 1000 for compartment 1 and 10,000 for compartment 2. Cell migration tends to equalize these, and since the uninfected cell death rate is low ($\mu = 0.001$), this starts to occur at low values of cell migration. At $M = 0.001$, for example, $\hat{n}_1 = 4000$ and $\hat{n}_2 = 7000$, a fourfold increase for compartment 1. By $M = 0.2$, \hat{n}_1 is nearly 5400, close to its maximum value of 5500 (when the two compartments are equalized), so further increase in M no longer has much effect on uninfected cell numbers. At higher rates of cell migration, movement of infected cells into the compartment with the higher viral clearance rate begins to be more important, and we again see a drop in μ'_{crit} as cell migration increases past this threshold amount.

If we allow the ratio between the two clearance rates to vary, we see that increasing the viral clearance rate in one compartment while holding the other constant makes persistent infection less likely. Fig. 4 shows the number of uninfected cells, infected cells, and virus in both compartments at equilibrium in the case for which μ'_2 is held constant ($\mu'_2 = 10$) but μ'_1 is increased. As compartment 1 becomes less hospitable to the virus, the equilibrium numbers of infected cells and virus decreases, eventually dipping below 1.

The death rate of infected cells (μ^*) has no effect on viral increase when rare in the absence of cell migration

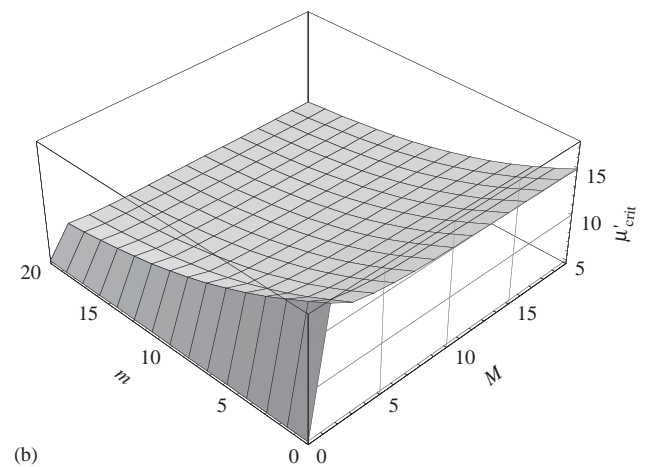
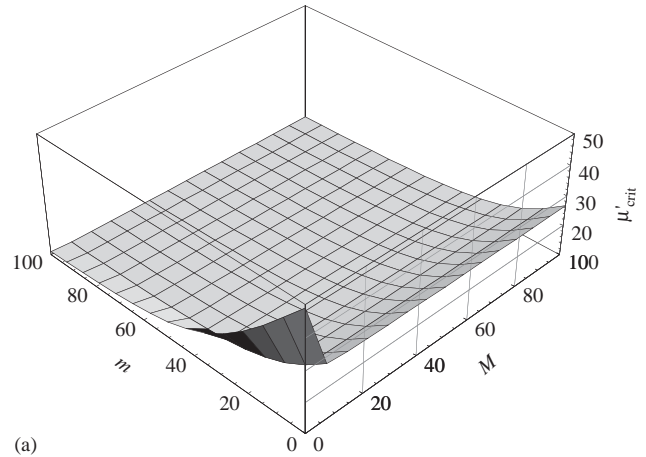


Fig. 3. Critical value for viral clearance rates (μ'_{crit}) for two-compartment, one-cell type model, where $\mu'_2 = 10\mu'_1$; values of μ'_1 below the surface allow for infection. Migration is symmetric and assumed equal for uninfected and infected cells ($m_1 = m_2 = m$ and $M_1 = M_2 = M_1^* = M_2^* = M$). (a) Only viral clearance rates differ between compartments. Parameter values are $\lambda_1 = \lambda_2 = 10$, $v_1 = v_2 = 50$, $\mu_1 = \mu_2 = 0.001$, $\mu_1^* = \mu_2^* = 1$, and $\beta_1 = \beta_2 = 10^{-4}$. Both viral and cell migration rates range from 0 to 100. (b) Both viral clearance rates and uninfected cell input rates differ between compartments. Parameters are as in part (a), except that $\lambda_1 = 1$ and $\lambda_2 = 10$. Both viral and cell migration rates range from 0 to 20.

(see Eq. (8)), and with cell migration, the critical value for infected cell death rate (μ^*_{crit}) is proportional to the cell migration rate. We see this in Fig. 5, where, for any given value of viral migration (m), the value of μ^*_{crit} is a linear and increasing function of the cell migration rate (M).

Isocline portrayal of invasion: viral migration alone. We present numerical results above for systems with both cell and virion migration. If we restrict ourselves to systems with only one type of migration, we can in many cases solve for conditions allowing viral persistence analytically, and for two compartments, can display fairly general results graphically using isoclines. We will first consider virion migration. To characterize the conditions for viral infection, it is useful to plot the

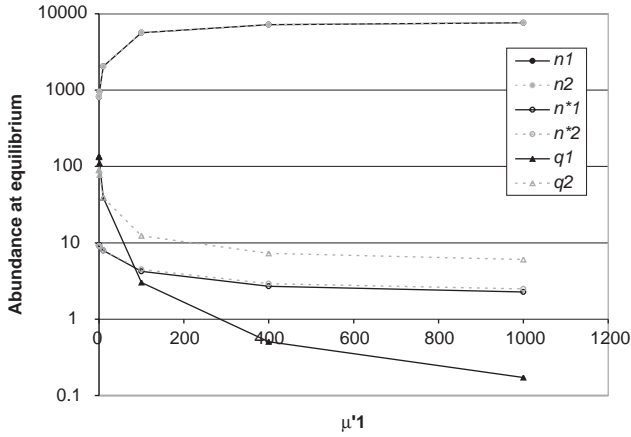


Fig. 4. Final equilibrium numbers of uninfected cells, infected cells, and virions versus viral clearance rate in compartment 1 (viral clearance rate in compartment 2 held constant). Parameter values are $\lambda_1 = \lambda_2 = 10$, $v_1 = v_2 = 50$, $\mu_1 = \mu_2 = 0.001$, $\mu_1^* = \mu_2^* = 1$, $\beta_1 = \beta_2 = 10^{-4}$, and $\mu_2' = 10$. Migration is symmetric and assumed equal for uninfected and infected cells ($m_1 = m_2 = m = 10$ and $M_1 = M_2 = M_1^* = M_2^* = M = 10$). Numerical iterations are begun with equal numbers of uninfected cells ($n_1 = n_2 = 10^4$), the levels of infected cells set to zero ($n_1^* = n_2^* = 0$), and the number of virions equal to 10 ($q_1 = q_2 = 10$).

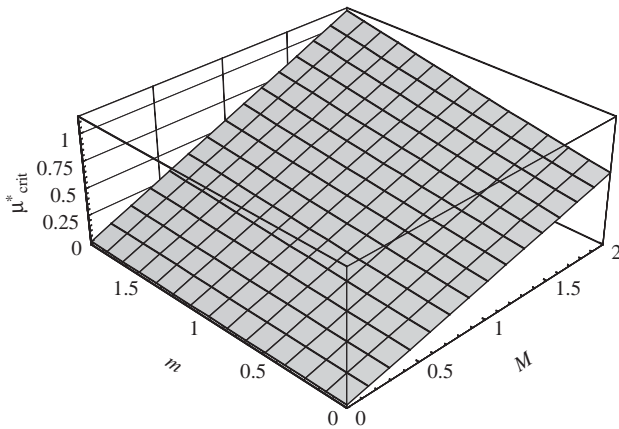
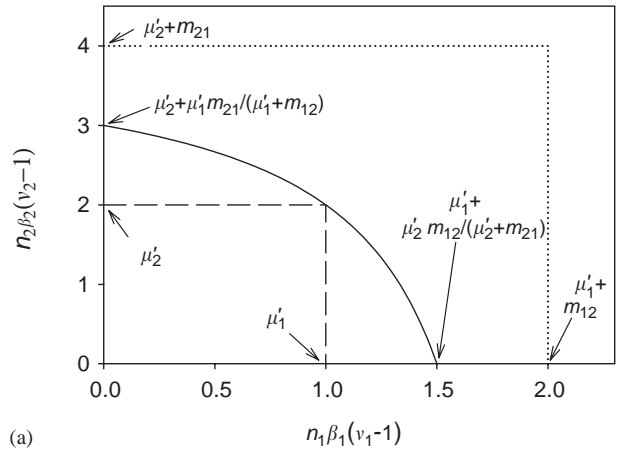
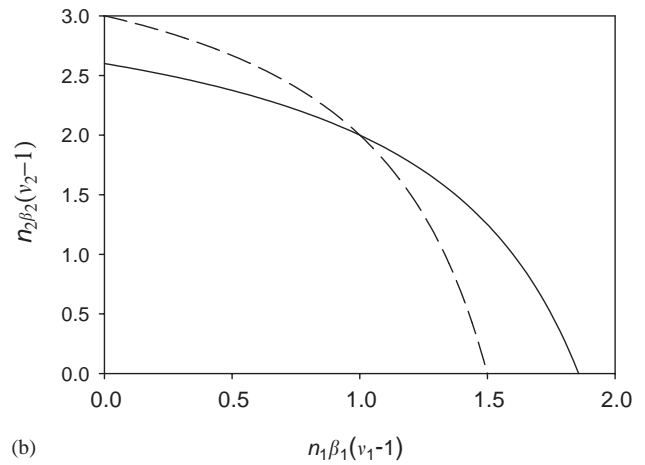


Fig. 5. Critical value for death rate of infected cells (μ_{crit}^*) for two-compartment, one-cell type model; values of μ_{crit}^* below the surface allow for infection. Parameter values are $\lambda_1 = \lambda_2 = 10$, $v_1 = v_2 = 50$, $\mu_1 = \mu_2 = 0.001$, $\mu_1' = 1$, $\mu_2' = 10$, and $\beta_1 = \beta_2 = 10^{-4}$. Migration is symmetric and assumed equal for uninfected and infected cells ($m_1 = m_2 = m$ and $M_1 = M_2 = M_1^* = M_2^* = M$). Both viral and cell migration rates range from 0 to 2. In the absence of cell migration ($M = 0$), there is no effect of infected cell death rate on the conditions for viral increase when rare; with cell migration, μ_{crit}^* is proportional to the cell migration rate.

inequality given in Eq. (8a) (which determines the boundary for infection) in the $\hat{n}_1\hat{n}_2$ -plane (see Fig. 6). The boundary is an isocline (line of zero virus growth) and the virus increases when rare for points, (\hat{n}_1, \hat{n}_2) , above and to the right of the isocline. The inequality in Eq. (8a) bounds the region between two branches of a hyperbola. The inequalities given in Eqs. (8b) and (8c) ensure that it is the lower branch that determines the



(a)



(b)

Fig. 6. (a) Zero-virus growth isoclines for two-compartment, one-cell-type model. Virus increases when rare in the area above and to the right of an isocline. The dashed line is the isocline in the limiting case of no migration in either direction (each compartment isolated). The solid line is an isocline with positive migration in both directions, which is the lower branch of a hyperbola, the asymptotes of which are indicated by the dotted lines. (b) Effect of asymmetrical migration. The solid line is an isocline for equal migration rates between compartments, while the dashed line has increased migration from compartment 2 to 1 and decreased migration from 1 to 2. Parameters for the solid line are $\mu_1' = 1$, $\mu_2' = 2$, $m_{12} = m_{21} = 1.5$. For the dashed line, clearance rates are the same, but $m_{12} = 1$, $m_{21} = 2$ [same as solid line in (a)].

invasion boundary. Since \hat{n}_i, β_i and v_i all appear together in Eq. (8), instead of density we can use as axes $\hat{n}_i\beta_i(v_i - 1)$, in which case the plot can be used to indicate the invasion conditions on \hat{n}_i, β_i or $v_i - 1$ given the other two are fixed, by simply dividing the axes by the fixed values. (We assume both v_1 and $v_2 > 1$ in the following discussion of isoclines, unless otherwise noted.) As the migration rates approach zero, the isocline approaches the segments of the lines $\hat{n}_i\beta_i(v_i - 1) = \mu_i'$ ($i = 1, 2$) to the left and below their intersection, which are indicated by the dashed lines in Fig. 8a. This is the nearest isocline can be to the origin, and therefore zero virion migration makes increase of the virus when rare easiest.

Of course, this assumes that the virus is present at a low level in each compartment. If only one of the migration rates (m_{12} or m_{21}) is zero, the segment of the isocline for the source compartment is shifted in the positive direction by the migration rate (it is more difficult for the virus to be sustained in the source due to outflow), while the other segment is unaffected. If there is positive migration in both directions, the isocline is the lower branch of the hyperbola given by Eq. (8a). This isocline is the solid line in Fig. 6a [which always goes through the point (μ'_1, μ'_2)] and the asymptotes are the dotted lines.

The isoclines intersect the axes at $\hat{n}_i\beta_i(v_i - 1) = \mu'_i + (\mu'_k m_{ik}/(\mu'_k + m_{ki}))$. If in one compartment (denoted k) the number of uninfected cells (or infection rate or net burst size) approaches 0, then for the other compartment (i), the left-hand side (LHS) of this equation must be greater than the right-hand side (RHS) for the virus to increase. The RHS is the clearance rate from compartment i , plus the migration rate from i to k multiplied by the probability that the virus in compartment k is cleared before it migrates back to i (since by assumption there are no cells in k to infect). The RHS is therefore the effective clearance rate from the system.

The asymptotes of the isocline are given by $\hat{n}_i\beta_i(v_i - 1) = \mu'_i + m_{ik}$. If the migration rates both increase, the asymptotes move further out and the isocline becomes straighter, approaching a straight line as the migration rates approach infinity. If the migration rates are equal and approach infinity, the intercepts are at $\hat{n}_i\beta_i(v_i - 1) = \mu'_i + \mu'_k$, and the equation of the isocline is $\hat{n}_i\beta_i(v_i - 1) + \hat{n}_k\beta_k(v_k - 1) = \mu'_i + \mu'_k$. The isocline always goes through (μ'_1, μ'_2) and is concave toward the origin; therefore, making it straighter means moving it outward, and so increasing virion migration makes viral increase more difficult. The reason is that with higher migration, there is a net flow of virus from tissues with a high inherent growth rate for the virus, to compartments with a lower growth rate. This reduces the average growth over both compartments combined.

For the special case in which both compartments are equivalent, so that $\hat{n}_1 = \hat{n}_2 = \hat{n}$, $\mu'_1 = \mu'_2 = \mu'$, $v_1 = v_2 = v$, $\beta_1 = \beta_2 = \beta$, the conditions in Eq. (8) reduce to

$$\hat{n} > \frac{\mu'}{\beta(v - 1)} \tag{12}$$

This is the same condition for increase as that for each compartment with uncoupled compartments (relation 10). The isoclines will vary with migration rates, but by assuming other parameters are equal in the two compartments, we restrict ourselves to a diagonal line, which intersects the isocline at the point (μ', μ') .

As mentioned above, with no migration, the isoclines are perpendicular lines (dashed lines in Fig. 6a), while with increased symmetric migration, the isocline tends to become straighter. Fig. 6b shows the effect of increasingly asymmetrical migration. The solid line is

for equal migration rates, while the dashed line has the same total migration rate, but with migration from compartment 2 to 1 higher, and migration in the reverse direction lower. The lines cross at (μ'_1, μ'_2) . Above and to the right of this point, both compartments satisfy (10) and the virus can increase when rare for any migration rates, while below and to the left of this point, neither compartment satisfies (10) and the virus can not increase when rare for any migration rate. Migration rates only matter in the other two regions: below and to the right of the intersection, relation (10) is satisfied for compartment 1 (to the right of μ'_1) but not for compartment 2 (below μ'_2). Compartment 1 is therefore more favorable for the virus, since it can increase when rare in an isolated compartment 1 while not for an isolated compartment 2. In this region, the dashed isocline is closer to the origin, so viral increase is easier. The migration rate into compartment 1 was increased from the solid to the dashed line. So viral increase is easier with increased asymmetric migration into the “better” compartment (the compartment that can support the virus in isolation).

For the region above and to the left of (μ'_1, μ'_2) , compartment 2 satisfies (10) while compartment 1 does not, so the migration rate into the better compartment is decreased, and the dashed line is further out, making viral increase more difficult. If flow out of a compartment is fast compared to flow into that compartment, virions spend less time, on average, in that compartment. If that compartment is the one in which the virus could persist alone, then this increase in movement out of the “better” compartment makes viral increase more difficult. (If the virus could persist alone in each compartment, then the virus can increase when rare, regardless of migration.)

We have assumed above that burst sizes are greater than one. However, one can imagine situations for which $v_i < 1$, so that cells act as a virion “sink.” For example, infected cells of a particular type might be removed by the immune system prior to lysis. In this case, an increase in uninfected cells of this type will actually make viral persistence less likely. If $v_i < 1$ in one compartment, the isocline is still hyperbolic, but one of the asymptotes is negative. This gives the isocline a positive slope in the first quadrant, reflecting the fact that increase in virus becomes more difficult as the number of uninfected cells increases in the compartment with $v_i < 1$.

If condition (8) is not satisfied, the virus cannot increase when rare and the infection fails, leaving only uninfected cells (so $q_i = 0$, $n_i^* = 0$, and $n_i = \lambda_i/\mu_i$). Numerical studies suggest that when this condition is not satisfied, any starting viral population configuration will tend towards extinction. Biologically, note that the above condition for invasion assumed that healthy, susceptible cells are at their carrying capacities. If virus

is present at non-trivial abundances, there will be fewer susceptible cells than possible at carrying capacity, and the rate of new infections (and hence per capita growth rate of the virus) should thus be depressed. This observation suggests that if the “edge” equilibrium is locally stable (i.e., the virus cannot increase when rare), the equilibrium is also globally stable (see Diekmann et al., 1990).

Isocline portrayal of invasion: cell migration alone. With migrating cells, the isocline equation (obtained from the conditions for increase of virus when rare) can be written as

$$\left[1 + \frac{M_{12}^*}{\mu_1^*} - \frac{v_1 \beta_1 \hat{n}_1}{\mu_1 + \beta_1 \hat{n}_1} \right] \left[1 + \frac{M_{21}^*}{\mu_2^*} - \frac{v_2 \beta_2 \hat{n}_2}{\mu_2 + \beta_2 \hat{n}_2} \right] < \frac{M_{12}^* M_{21}^*}{\mu_1^* \mu_2^*}.$$

Although this is not a parabolic function of uninfected cell number (as the isocline was with migrating virions), it has a similar shape for many parameter values. If both migration rates (M_{12}^*, M_{21}^*) are 0, the isocline consists of horizontal and vertical line segments, which are identical to those with migrating virions (since with migration rates set to 0, there is no migration in either case). With both migration rates positive (and not too large), the isocline becomes curved and concave toward the origin, and always passes through the corner point of the no-migration isocline (as with virion migration). However, for sufficiently high migration rates ($M_{12}^*/[\mu_1^*(v_1 - 1)] + M_{21}^*/[\mu_2^*(v_2 - 1)] = 1$), the isocline becomes a straight line. For higher migration rates the isocline becomes concave away from the origin. This concavity is especially pronounced for low burst sizes. For sufficiently low burst sizes, the isocline has a horizontal or vertical asymptote.

These qualitative differences with the migrating-virion isocline can be explained by the fact that uninfected cell numbers in the above expression appear in terms that saturate with increasing cell numbers. Therefore, there are diminishing effects of increasing cell numbers. If the isocline is plotted on the axes $x_i = v_i \beta_i \hat{n}_i / (\mu_i + \beta_i \hat{n}_i)$, then it has a parabolic form with asymptotes $x_1 = 1 + M_{12}^*/\mu_1^*$ and $x_2 = 1 + M_{21}^*/\mu_2^*$, and always passes through the point (1,1). However, we are interested in the isocline as a function of \hat{n}_i (we will scale these axes using β_i and μ_i^*). Solving the x_i expression gives $\beta_i \hat{n}_i / \mu_i^* = x_i / (v_i - x_i)$. As long as $x_i \ll v_i$, the cell number axis is just the x_i axis rescaled. However, this inequality is increasingly violated as x_i increases, and this leads to the x_i axis being increasingly stretched to higher values. Therefore, relative to a parabola, the isocline for cell movement has higher values on each axis moved relatively further away from the origin. This accounts for the fact that, instead of approaching a straight line at high migration rates as with virion migration, the

isocline becomes concave away from the origin, especially at low v_i .

Setting $M_{12}^* = M_{21}^* = M^*$, in the limit as $M^* \rightarrow \infty$, the axis intercepts approach $\beta_i \hat{n}_i / \mu_i^* = 2 / (\mu_i^* v_i / \bar{\mu}^* - 2)$, where $\bar{\mu}^* = (\mu_1^* + \mu_2^*) / 2$. For sufficiently low burst size, the denominator becomes negative and the corresponding intercept becomes infinite. This indicates that the isocline has a vertical or horizontal asymptote.

2.4. Two compartment model with a multiple cell types per compartment

Assume two compartments for the model in Eqs. (1)–(3). Using the same method as used in Appendix A and B, we can find the conditions necessary for the virus to increase when rare. First, consider the case of viral migration alone. Let the net rate of virion loss for a compartment i (in the absence of migration into it) be

$$B_i = \mu_i' + m_{ik} - \sum_j \hat{n}_{ji} \beta_{ji} (v_{ji} - 1) \tag{13}$$

where k is the other compartment, and $\hat{n}_{ji} = \lambda_{ji} / \mu_{ji}$ is the equilibrium number of uninfected cells of type j in compartment i in the absence of infection. If $B_i < 0$ for a compartment, the virus in that compartment can increase when rare even in the absence of any virion flow from the other compartment. If $B_i > 0$ for both compartments, the virus can still increase when rare if $B_1 B_2 < m_{12} m_{21}$. So the virus increases when rare if either

$$\left[\mu_1' + m_{12} - \sum_j \hat{n}_{j1} \beta_{j1} (v_{j1} - 1) \right] \times \left[\mu_2' + m_{21} - \sum_j \hat{n}_{j2} \beta_{j2} (v_{j2} - 1) \right] < m_{12} m_{21}, \tag{14}$$

or either factor in brackets is negative. This is the same condition as Eq. (8), except that the $\hat{n}_i \beta_i (v_i - 1)$ terms in Eq. (8) are now replaced by the corresponding sums over all cell types.

We can follow similar reasoning and find that the condition for viral increase when rare under cell migration alone is satisfied if

$$\left[\mu_1^* + M_{12}^* - \frac{\mu_1^* \sum v_{j1} \beta_{j1} \hat{n}_{j1}}{\mu_1' + \sum \beta_{j1} \hat{n}_{j1}} \right] \times \left[\mu_2^* + M_{21}^* - \frac{\mu_2^* \sum v_{j2} \beta_{j2} \hat{n}_{j2}}{\mu_2' + \sum \beta_{j2} \hat{n}_{j2}} \right] < M_{12}^* M_{21}^* \tag{15}$$

or if either factor in brackets is negative. This is the same condition as Eq. (9) except that, similarly to the case for viral migration alone, the $v_i \beta_i \hat{n}_i$ terms in Eq. (9) are now replaced by the corresponding sums over all cell types. This result requires that migration rates and cell death rates must be the same for all cell types (although they may differ by compartment).

If we define the total number of cells in compartment i as $n_{Ti} = \sum_j \hat{n}_{ji}$, Eqs. (14) and (15) can be rewritten as

$$[\mu'_1 + m_{12} - n_{T1}E\{\beta_1(v_1 - 1)\}] \times [\mu'_2 + m_{21} - n_{T2}E\{\beta_2(v_2 - 1)\}] < m_{12}m_{21}, \tag{16}$$

$$\left[\mu_1^* + M_{12}^* - \frac{\mu_1^* n_{T1} E\{\beta_1 v_1\}}{\mu_1^* + n_{T1} E\{\beta_1\}} \right] \times \left[\mu_2^* + M_{21}^* - \frac{\mu_2^* n_{T2} E\{\beta_2 v_2\}}{\mu_2^* + n_{T2} E\{\beta_2\}} \right] < M_{12}^* M_{21}^*, \tag{17}$$

where the expectations, $E\{\cdot\}$, are taken over the distribution of uninfected cell types in each of the two compartments. This allows the above isocline analysis of viral invasion to be extended to multiple cell types, by replacing cell numbers, \hat{n}_i , with total numbers of cells, n_{Ti} , and replacing $\beta_i(v_i - 1)$, $\beta_i v_i$ and β_i with their expected values over the cell types in the two compartments. The first two of these expectations can be rewritten as $E\{\beta_i(v_i - 1)\} = E\{\beta_i\}E\{v_i - 1\} + Cov[\beta_i, v_i]$ and $E\{\beta_i v_i\} = E\{\beta_i\}E\{v_i\} + Cov[\beta_i, v_i]$. This shows the importance of the sign of the covariance between the infection rate and the burst size (across cell types within a compartment) on the conditions for viral persistence. As an example, imagine a cell type that is rare in a particular compartment and that has a high infection rate combined with a low average burst size. This could be due to the frequent removal of this cell type by the immune system prior to lysis. Such a cell would have a negligible effect on the total number of cells, but could cause the covariance term to be negative, making viral persistence less likely.

3. Discussion

For the majority of the cases we have examined, symmetric migration between compartments makes establishment of infection more difficult than it would be in the absence of migration. The analyses of virion migration alone and cell migration alone show that establishment of infection is most likely (occurs for the largest region of the parameter space) without migration. Within-host heterogeneity combined with movement among compartments hampers the initial phase of establishment of a viral population. This result is an example of a general phenomenon that has been previously identified in population ecology: in spatially varying but temporally constant environments, symmetric movement between distinct habitats almost always lowers the initial growth rate of invading populations (Holt, 1985). It contrasts our previous finding that the inclusion of multiple cell types within a single spatial compartment (cellular population structure) increases the likelihood of persistent infection (Kelly et al., 2003). The result that increased migration

generally hinders persistence may contribute to the tissue specificity of some viruses (Flint et al., 2000, Chapter 4). If the virus can avoid movement among tissues, growth in preferred tissues or compartments can be fostered. Of course, this tendency may be limited by the extent to which pathogens can control their movement among compartments.

There are two important caveats to this generalization. First, consider a virus that is initially entirely restricted to a single compartment by virtue of the biology of transmission (for example, viruses associated with sexually transmitted diseases). If this compartment is unfavorable (e.g., host cell number is less than the threshold value), successful infection depends on the virus migrating to other compartments with more favorable growth conditions. Second, while we have observed no instances of sustained oscillations, many parameter combinations produced high-amplitude damped oscillations on the approach to equilibrium values (see also Callaway and Perelson, 2002, Section 5.1). The deterministic model does not take into account stochastic effects. Large amplitude oscillations may cause the viral population to die out early in infection, well before equilibrium is reached. Not surprisingly, increased migration between compartments decreases the dissipation time of the oscillations. Fig. 7 illustrates the effect of adding viral migration on infected cell and viral population fluctuations during initial establishment. In this example, compartment 2 has a higher viral clearance rate ($\mu'_1 = 0.1, \mu'_2 = 1$); with no migration between compartments, both the numbers of infected cells and virus show damped oscillations as they approach their equilibrium values for compartment 2 ($m = 0$, Fig. 7a). Both the magnitude of oscillations and the time until oscillations are damped are decreased substantially by allowing a modest amount of migration between the compartments ($m_{12} = m_{21} = 0.5$ in Fig. 7b). Thus, migration may tend to reduce average growth rate, yet nonetheless facilitate establishment of an infection by reducing the length of time during which sustained oscillations are observed. We intend to examine the stochastic dimensions of both of these aspects of establishment elsewhere.

Another consideration for spatially structured models of infection is the effect of compartment “size” on the type of viral transmission. We track numbers of cells and virus, and use a density-dependent transmission function [rather than a frequency-dependent transmission function, see discussion in McCallum et al. (2001) and Begon et al. (2002)]. Thus, the contact rate increases with the overall numbers of cells, and also increases with the density for constant volume. For a one-compartment model, the fact that we do not explicitly consider compartment size can be dealt with by assuming that our infection constant β is in fact equivalent to an infection constant per unit volume (that is $\beta = \beta' / V$,

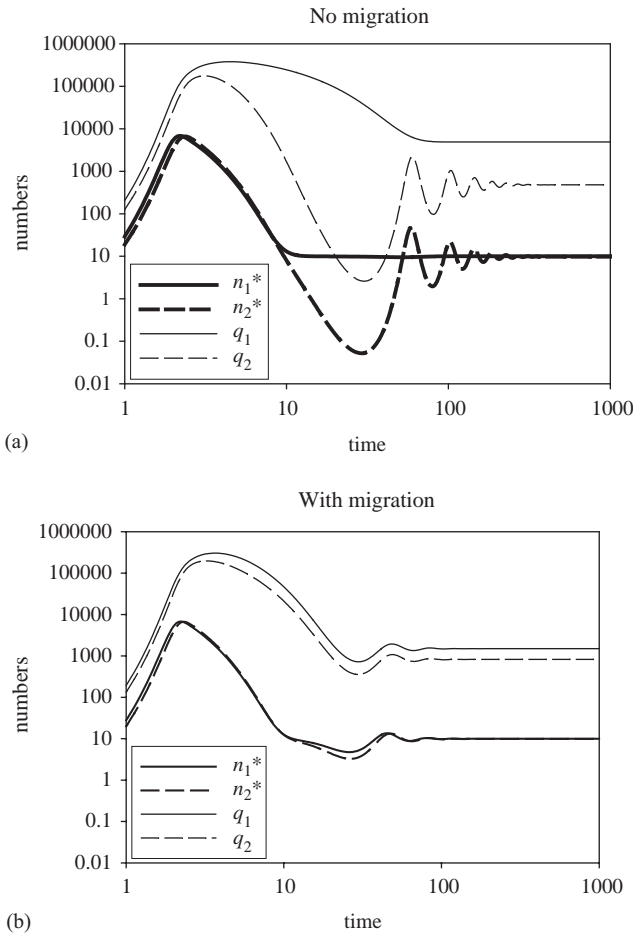


Fig. 7. Approach to equilibrium for two-compartment, one-cell-type model. Parameters are $\lambda_1 = \lambda_2 = 10$, $\mu_1 = \mu_2 = 0.001$, $\mu_1^* = \mu_2^* = 1$, $\beta_1 = \beta_2 = 0.0001$, $v_1 = v_2 = 50$, $\mu'_1 = 0.1$, $\mu'_2 = 1$. The system was started with uninfected cells at their no-infection equilibria, infected cells at 0, and virion abundances at 1 in each compartment. (a) No migration. (b) $m_{12} = m_{21} = 0.5$. Note that plots are given on a log–log scale.

where V is the volume) and setting that volume to the compartment size (Begon et al., 2002). In moving from the one-compartment model to a model with two compartments, we have generally assumed that $\beta_1 = \beta_2 = \beta$. We have, in essence, doubled the available volume within the host by adding another compartment of the same size; this corresponds to increasing the available “habitat” for the virus by allowing the virus to occupy another compartment (see Appendix C). However, when considering more than one compartment, the question arises as to how different sized compartments would affect transmission and migration. If there are different infection constants in each compartment (β_i for compartment i), we can define each infection constant relative to the volume of the compartment. We will consider the effects of compartment size on migration rates in future extensions of the model considered here.

Our model does not include two important possible forms of density dependence. First, input of uninfected cells is assumed to be constant and independent of local cell or viral abundances. Second, we do not include density-dependent immunological and other defensive responses by the host, which would be expected to affect the viral clearance rate and the death rate of infected cells.

While we have focused on the dynamical consequences of internal structure, it is important to note that spatial structuring can also profoundly influence evolutionary change (Barton and Whitlock, 1997; Wade and Goodnight, 1998). It is an implicit component of models of social evolution involving fitness-determining interactions between genetically related individuals (Kelly, 1992; Frank, 1998). Spatial structure can be important even with spatially uniform selection. In particular, spatial structure slows the rate at which a uniformly favorable allele becomes fixed (Whitlock and Barton, 1997). Spatial structure critically influences the importance of genetic drift: a species which is subdivided into spatially localized populations with extinction and recolonization has a different variance effective population size than an undivided species with an equal total number of individuals (Whitlock and Barton, 1997). Effective size also governs the importance of drift relative to deterministic evolutionary forces such as selection. This directly affects, for example, the probability that new favorable mutations are fixed (Ewens, 1979). The processes described above may help to explain why some estimates of effective population size of HIV are surprisingly small (Leigh Brown, 1997).

Finally, recent studies of evolution in spatially heterogeneous environments suggest that selection tends to be biased towards habitats with the greatest numbers of individuals or in which fitness or productivity is highest (Holt, 1996; Kawecki, 2000). Our theoretical studies provide an essential theoretical foundation for examining comparable phenomena in an internally heterogeneous host environment. Migration in our system creates a series of induced “sources” and “sinks,” where realized viral abundance is depressed in compartments that in isolation would experience greater viral abundance, and the virus there correspondingly enjoy greater local growth rates than virus in other compartments. Moreover, migration can maintain viral populations in compartments where extinction would be expected, were those compartments to be isolated. Heterogeneities and asymmetries in space, in abundance and fitness can lead to asymmetries in directions of natural selection (e.g., Holt, 1996). We expect such asymmetries to play potentially important roles in constraining or facilitating adaptive evolution of viruses to the internally heterogeneous host environment.

Acknowledgments

We would like to thank three anonymous reviewers for their helpful comments. This work was supported by NIH grant 5 R01 GM60792-04; R.D.H. and M.B. also thank the University of Florida Foundation for support.

Appendices A, B and C. Supplementary data

The online version of this article contains additional supplementary data. Please visit [doi:10.1016/j.jtbi.2004.08.023](https://doi.org/10.1016/j.jtbi.2004.08.023)

References

- Andreasen, V., Christiansen, F.B., 1989. Persistence of an infectious disease in a subdivided population. *Math. Biosci.* 96, 239–253.
- Antia, R., Levin, B.R., May, R.M., 1994. Within-host population dynamics and the evolution and maintenance of microparasite virulence. *Am. Nat.* 144, 457–472.
- Barton, N.H., Whitlock, M.C., 1997. The evolution of metapopulations. In: Hanski, I.A., Gilpin, M.E. (Eds.), *Metapopulation Biology: Ecology, Genetics and Evolution*. Academic Press, San Diego, pp. 183–214.
- Begon, M., Bennett, M., Bowers, R.G., French, N.P., Hazel, S.M., Turner, J., 2002. A clarification of transmission terms in host-microparasite models: numbers, densities, and areas. *Epidemiol. Infect.* 129, 147–153.
- Bonhoeffer, S., Coffin, J.M., Nowak, M.A., 1997. Human immunodeficiency virus drug therapy and virus load. *J. Virol.* 71, 3275–3278.
- Callaway, D.S., Perelson, A.S., 2002. HIV-1 infection and low steady state viral loads. *Bull. Math. Biol.* 64, 29–64.
- Cuevas, J.M., Moya, A., Elena, S.F., 2003. Evolution of RNA virus in spatially structured heterogeneous environments. *J. Evol. Biol.* 16, 456–466.
- Delassus, S., Cheyner, R., Wain-Hobson, S., 1992. Nonhomogeneous distribution of human immunodeficiency virus type 1 proviruses in the spleen. *J. Virol.* 66, 5642–5645.
- Diekmann, O., Heesterbeek, J.A.P., Metz, J.A.J., 1990. On the definition and the computation of the basic reproduction ratio R_0 in models for infectious diseases in heterogeneous populations. *J. Math. Biol.* 28, 365–382.
- Dobson, A., Fofopoulos, J., 2001. Emerging infectious pathogens of wildlife. *Philos. Trans. R. Soc. London B* 356, 1001–1012.
- Epstein, L.G., Kuiken, C., Blumberg, B.M., Hartman, S., Sharer, L.R., Clement, M., Goudsmit, J., 1991. HIV-1 V3 domain variation in brain and spleen of children with AIDS: tissue-specific evolution within host-determined quasispecies. *Virology* 180, 583–590.
- Essunger, P., Perelson, A.S., 1994. Modeling HIV infection of CD4+ T-cell subpopulations. *J. Theor. Biol.* 170, 367–391.
- Ewens, W.J., 1979. *Mathematical Population Genetics*. Springer, Berlin.
- Flint, S.J., Enquist, L.W., Krug, R.M., Racaniello, V.R., Skalka, A.M. (Eds.), 2000. *Principles of Virology: Molecular Biology, Pathogenesis, and Control*. ASM Press, Washington, DC.
- Frank, S.A., 1998. *Foundations of Social Evolution*. Princeton University Press, Princeton, NJ.
- Fulford, G.R., Roberts, M.G., Heesterbeek, J.A.P., 2002. The metapopulation dynamics of an infectious disease: tuberculosis in possums. *Theor. Popul. Biol.* 61, 15–29.
- Hanski, I.A., Gilpin, M.E. (Eds.), 1997. *Metapopulation Biology*. Academic Press, San Diego.
- Hassell, M.P., Comins, H.N., May, R.M., 1994. Species coexistence and self-organizing spatial dynamics. *Nature* 370, 290–292.
- Herz, A.V., Bonhoeffer, S., Anderson, R.M., May, R.M., Nowak, M.A., 1996. Viral dynamics *in vivo*: limitations on estimates of intracellular delay and virus decay. *Proc. Natl. Acad. Sci. USA* 93, 7247–7251.
- Hlavacek, W.S., Stilianakis, N.I., Perelson, A.S., 2000. Influence of follicular dendritic cells on HIV dynamics. *Philos. Trans. R. Soc. London B* 355, 1051–1058.
- Holt, R.D., 1985. Population dynamics in two-patch environments: Some anomalous consequences of an optimal habitat distribution. *Theor. Popul. Biol.* 28, 181–208.
- Holt, R.D., 1996. Demographic constraints in evolution: towards unifying the evolutionary theories of senescence and niche conservatism. *Evol. Ecol.* 10, 1–11.
- Holt, R.D., 2000. A biogeographical and landscape perspective on within-host infection dynamics. In: Bell, C.R., Brylinsky, M., Johnson-Green, P. (Eds.), *Proceedings of the 8th International Symposium of Microbial Ecology*. Atlantic Canada Society for Microbial Ecology, Halifax, Canada, pp. 583–588.
- Holt, R.D., Hassell, M.P., 1993. Environmental heterogeneity and the stability of host-parasitoid interactions. *J. Anim. Ecol.* 62, 89–100.
- Horn, R.A., Johnson, C.A., 1985. *Matrix Analysis*. Cambridge University Press, Cambridge.
- Kawecki, T.J., 2000. Adaptation to marginal habitats: contrasting influence of the dispersal rate on the fate of alleles with small and large effects. *Proc. R. Soc. Biol. Sci. Ser. B* 267, 1315–1320.
- Kelly, J.K., 1992. Kin selection in density regulated populations. *J. Theor. Biol.* 157, 447–461.
- Kelly, J.K., 1996. Replication rate and evolution in the human immunodeficiency virus. *J. Theor. Biol.* 180, 359–364.
- Kelly, J.K., Williamson, S., Orive, M.E., Smith, M.S., Holt, R.D., 2003. Linking dynamical and population genetic models of persistent viral infection. *Am. Nat.* 162, 14–28.
- Kepler, T.B., Perelson, A.S., 1998. Drug concentration heterogeneity facilitates the evolution of drug resistance. *Proc. Natl. Acad. Sci. USA* 95, 11514–11519.
- Kirschner, D., 2001. Reconstructing microbial pathogenesis. *ASM News* 67, 566–573.
- Kirschner, D.E., Mehr, R., Perelson, A.S., 1998. Role of the thymus in pediatric HIV-1 infection. *J. Acquir. Immune Defic. Syndr. Hum. Retrovirol.* 18, 95–109.
- Leigh Brown, A.J., 1997. Analysis of HIV-1 *env* gene sequences reveals evidence for a low effective number in the viral population. *Proc. Natl. Acad. Sci. USA* 94, 1862–1865.
- Lipsitch, M., Levin, B.R., 1997. The population dynamics of antimicrobial chemotherapy. *Antimicrob. Agents Chemother.* 363–373.
- Lipsitch, M., Levin, B.R., 1998. Population dynamics of tuberculosis treatment: mathematical models of the roles of non-compliance and bacterial heterogeneity in the evolution of drug resistance. *Int. J. Tuberc. Lung. Dis.* 2, 187–199.
- May, R.M., Anderson, R.M., 1990. Parasite–host coevolution. *Parasitology* 100, S89–S101.
- May, R.M., Gupta, S., McLean, A.R., 2001. Infectious disease dynamics: what characterizes a successful invader? *Philos. Trans. R. Soc. London B* 356, 901–910.
- McCallum, H., Barlow, N., Hone, J., 2001. How should pathogen transmission be modeled? *Trends Ecol. Evol.* 16, 295–300.
- McLean, A.R., Nowak, M.A., 1992. Competition between zidovudine-sensitive and zidovudine-resistant strains of HIV. *AIDS* 6, 71–79.

- Nelson, P.W., Murray, J.D., Perelson, A.S., 2000. A model of HIV-1 pathogenesis that includes an intracellular delay. *Math. Biosci.* 163, 201–215.
- Nelson, P.W., Perelson, A.S., 2002. Mathematical analysis of delay differential equation models of HIV-1 infection. *Math. Biosci.* 179, 73–94.
- Nowak, M.A., May, R.M., 2000. *Virus Dynamics: Mathematical Principles of Immunology and Virology*. Oxford University Press, Oxford.
- Palm III, W.J., 1983. *Modeling, Analysis and Control of Dynamic Systems*. Wiley, New York.
- Pang, S., Vinters, H.V., Akashi, T., O'Brien, W.A., Chen, I.S.Y., 1991. HIV-1 env sequence variation in brain tissues of patients with AIDS-related neurologic disease. *J. Acquir. Immune Defic. Syndr.* 4, 1082–1092.
- Perelson, A.S., 1989. Modeling the interaction of the immune system with HIV. In: Castillo-Chavez, C. (Ed.), *Mathematics and Statistical Approaches to AIDS Epidemiology*. Springer, Berlin, pp. 350–370.
- Perelson, A.S., Kirschner, D.E., De-Boer, R., 1993. Dynamics of HIV infection of CD4+ T cells. *Math. Biosci.* 114, 81–125.
- Perelson, A.S., Neumann, A.U., Markowitz, M., Leonard, J.M., Ho, D.D., 1996. HIV-1 dynamics *in vivo*: virion clearance rate, infected cell life-span, and viral generation time. *Science* 271, 1582–1586.
- Perelson, A.S., Essunger, P., Cao, Y., Vesonen, M., Hurely, A., Saksela, K., Markowitz, M., Ho, D.D., 1997. Decay characteristics of HIV-1 infected compartments during combination therapy. *Nature* 387, 188–191.
- Ribeiro, R.M., Lo, A., Perelson, A.S., 2002. Dynamics of hepatitis B virus infection. *Microbes Infect* 4, 829–835.
- Solé, R.V., Ferrer, R., González-García, I., Quer, J., Domingo, E., 1999. Red queen dynamics, competition, and critical points in a model of RNA virus quasispecies. *J. Theor. Biol.* 198, 47–59.
- Stekel, D.J., 1997. The role of inter-cellular adhesion in the recirculation of T lymphocytes. *J. Theor. Biol.* 186, 491–501.
- Tilman, D., 1994. Competition and biodiversity in spatially structured habitats. *Ecology* 75, 2–16.
- Tilman, D., Kareiva, P.M. (Eds.), 1997, *Spatial Ecology: The Role of Space in Population Dynamics and Interspecific Interactions*. Princeton University Press, Princeton, NJ.
- Tuckwell, H.C., Le Corfec, E., 1998. A stochastic model for early HIV-1 population dynamics. *J. Theor. Biol.* 195, 451–463.
- Verotta, D., Schaedeli, F., 2002. Non-linear dynamics models characterizing long-term virological data from AIDS clinical trials. *Math. Biosci.* 176, 163–183.
- Wade, M.J., Goodnight, C.J., 1998. The theories of Fisher and Wright in the context of metapopulations: when nature does many small experiments. *Evolution* 52, 1537–1553.
- Wang, T.H., Donaldson, Y.K., Brettler, R.P., Bell, J.E., Simmons, P., 2001. Identification of shared populations of human immunodeficiency virus type 1 infecting microglia and tissue macrophages outside the central nervous system. *J. Virol.* 75, 11686–11699.
- Whitlock, M.C., Barton, N.H., 1997. The effective size of a subdivided population. *Genetics* 146, 427–441.